Burdenko's Journal of Neurosurgery
2024, №6, pp. 54–62
https://doi.org/10.17116/neiro20248806154

A Novel Rat Glioblastoma 101/8 Model: A Comparative PET-CT Study with C6 Rat model

© I.N. PRONIN[1, 2], A.A. POSTNOV[1, 3], A.A. LIPENGOLTS[4], G.V. PAVLOVA[1, 5], A.V. REVISHCHIN[5], V.A. SKRIBITSKY[4], YU.A. FINOGENOVA[4], A.V. SMIRNOVA[4], K.E. SHPAKOVA[4], E.YU. GRIGORIEVA[4], YU.A. KOZLOVA[2, 6], A.I. ALEKSEEVA[1, 5, 7]

[1]Burdenko Neurosurgical Center, Moscow, Russia;
[2]Russian Medical Academy of Continuous Professional Education, Moscow, Russia;
[3]The Lebedev Physical Institute of the Russian Academy of Sciences, Moscow, Russia;
[4]Blokhin National Medical Research Center of Oncology, Moscow, Russia;
[5]Institute of Higher Nervous Activity and Neurophysiology, Russian Academy of SciencesMoscow, Russia;
[6]Botkin Hospital, Moscow, Russia;
[7]Avtsyn Research Institute of Human Morphology of Federal state budgetary scientific institution «Petrovsky National Research Centre of Surgery», Moscow, Russia

ABSTRACT

The development of new drugs in nuclear medicine for diagnosis or treatment (chemotherapy) of brain tumors, in particular gliomas, is inextricably linked with the use of tumor models in animals (usually rats).

Objective. To compare the widely used glioma cell model C6 and the new experimental tissue model of glioblastoma 101.8.

Material and methods. A comparison was made of the diagnostic and morphological characteristics of the presented glioma models in two groups of animals with intracranially implanted tissue strain of experimental glioblastoma 101.8 (*n*=4) and the C6 glioma cell line (*n*=4) throughout the tumor development cycle within the rat brain. To monitor the progress of tumor growth and development, each animal underwent repeated diagnostic studies using PET-CT with ^{18}F-FDG and ^{18}F-FET to assess the metabolic activity and volume of the tumor. Also MRI images were collected. After the end of data acquisition, a histological examination of the tumor was carried out.

Results. The tissue model of glioblastoma 101.8 demonstrated rapid growth and pronounced accumulation of the tracers in all animals during the tumor observation cycle. Formation of intratumoral necrosis and signs of disruption of the blood-brain barrier (BBB) were detected. In PET-CT studies of animals with a transplanted C6 tumor, no visible necrosis in the tumor structure was observed. Tumor growth was less rapid than in the case of model 101.8. The obtained morphological characteristics of 101.8 tumors transplanted into the rat brain demonstrated similar properties observed in real clinical conditions in patients with glioblastoma of the brain (necrosis, neovascularization, multiple pseudopalisade structures).

Conclusions. Tumor model 101.8 can be recommended for scientific research as it most closely reproduces the diagnostic and morphological features of a human glioblastoma.

Keywords: *glioma model 101.8, glioma model C6, micro-PET, glioblastoma, micro-CT with contrast agent, animal MRI.*

INFORMATION ABOUT THE AUTHOR:
Pronin I.N. — https://orcid.org/0000-0002-4480-0275
Postnov A.A. — https://orcid.org/0000-0003-2504-2090
Lipengolts A.A. — https://orcid.org/0000-0002-5631-9016
Pavlova G.V. — https://orcid.org/0000-0002-6885-6601
Revishchin A.V. — https://orcid.org/0000-0002-6007-6440
Skribitsky V.A. — https://orcid.org/0000-0003-2942-7895
Finogenova Yu.A. — https://orcid.org/0000-0002-5144-1039
Smirnova A.V. — https://orcid.org/0000-0003-0386-9732
Shpakova K.E. — https://orcid.org/0000-0003-0386-9732
Grigorieva E.Yu. — https://orcid.org/0000-0001-7726-7991
Kozlova Yu.A. — https://orcid.org/0000-0002-8026-5919
Alekseeva A.I. — https://orcid.org/0000-0002-0370-6477
Corresponding author: Postnov A.A. — e-mail: postnov.email@gmail.com

TO CITE THIS ARTICLE:
Pronin IN, Postnov AA, Lipengolts AA, Pavlova GV, Revishchin AV, Skribitsky VA, Finogenova YuA, Smirnova AV, Shpakova KE, Grigorieva EYu, Kozlova YuA, Alekseeva AI. A Novel Rat Glioblastoma 101/8 Model: A Comparative PET-CT Study with C6 Rat model *Burdenko's Journal of Neurosurgery*. 2024;88(6):54–62. (In Russ.). https://doi.org/10.17116/neiro20248806154

Introduction

Glioblastoma is the most malignant primary brain neoplasm. Despite a comprehensive approach (resection, chemo- and radiotherapy), the median survival is about 15 months.

Preclinical experimental studies are necessary for development of new diagnostic and therapeutic drugs for this disease. Most often, rats are used. Adequate animal models are a fundamental factor, since in vitro methods (with cell cultures, explants, etc.) and computer modeling are insufficient to predict clinical success of therapeutic drugs or techniques [1]. Cell lines of chemically induced tumors (in particular gliomas) are often used as models. These models are studied in vitro and after subcutaneous or intracranial implantation into the carrier/host animal. The most common models are C6 (Wistar rats), F98 and 9L (Fischer rats) [2, 3]. After implantation of 10^5—10^6 tumor cells into the brain, a node occurs, and this neoplasm may be visualized using specialized MR scanners and histological methods.

Experiments revealed certain disadvantages of these models including morphological differences from human glioblastoma, low tumor invasion, autologous immune reaction and low vascularization [4]. Another significant problem is serious difference between animal tumor models and human glioblastoma in their molecular genetic profile (significantly lower EGFR, TERT or MGMT expression) [5]. Therefore, searching for the model most fully reproducing characteristics of human glioblastoma remains relevant.

Positron emission tomography (PET) is currently used to assess tumor metabolism. Modern scanners allow analysis of small objects such as rats and mice using detector systems with high spatial resolution [6].

Experimental glioblastoma 101.8 is a tissue model of glioblastoma obtained by intracerebral passaging, i.e. sequential transplantation of chemically induced brain tumor from donor animal to recipient animal without cultivation in vitro [7]. It is believed that its histological characteristics are close to human glioblastoma [8, 9].

We compared phenotypic (CT, MRI, PET-CT) and morphological characteristics of tissue model 101.8 and cell model C6 to identify the most adequate model of glioblastoma.

Material and methods

Animals. We used 12 sexually mature male Wistar rats including 4 ones for revitalization of glioma 101.8 cells (weight 200—250 g). All animals were randomized into 2 groups with subsequent implantation of glioma C6 or 101.8.

Implantation of glioma 101.8. We obtained tissue glioblastoma 101.8 from collection of experimental tumors of nervous system and neural tumor cell lines of the Avtsyn Research Institute of Human Morphology.

Tissue glioblastoma 101.8 is stored as tissue fragments in cryogenic conditions at a temperature of –196^{0}C. To revitalize sample, we defrosted tissue and separated cryoprotectant through centrifugation. Suspension was implanted into animals under zoletil-xylazine anesthesia through scalp incision and trephination. The wound was sutured. Clinical symptoms developed after 14—20 days. Animals were euthanized in a CO_2 chamber. The tumor was removed under sterile conditions, crushed and implanted into experimental animals (0.8—1 million cells, EC-20 cell counter, Bio-Rad, USA). We implanted tumor cells into the right hemisphere (laterally and caudally 2 mm from bregma) to a depth of 4 mm from outer surface of skull. The wound was sutured.

Implantation of C6 glioma. We used C6 glioma cell line from the ATCC collection stored in the Laboratory of Neurogenetics and Developmental Genetics of the Institute of Higher Nervous Activity and Neurophysiology. Cells were defrosted, separated from cryoprotectant by centrifugation and cultured in DMEM/F12 medium (PanEco, Russia) with 10% fetal embryonic serum (Hyclone, USA) and L-glutamine (PanEco, Russia). For implantation, cells in log growth phase were detached from substrate using Trypsin-Versene solution (PanEco, Russia) and concentrated to 20 µl in Hanks' solution (PanEco, Russia). Implantation was carried out in similar manner into the left hemisphere.

All animals were under anesthetic sleep throughout further examinations (2% air mixture of isoflurane).

MRI was performed after 7, 14 and 18 days (Bruker BioSpec 7T animal scanner, Rheinstetten, Germany). Gadolinium 1.0 mmol/ml was injected into the tail vein at a dose of 0.4 mmol/kg. Analysis was started no later than 5 minutes after injection. T1-FLASH pulse sequence was the main imaging option. Total scanning time was 3 minutes.

MicroPET-CT. As soon as tumor reached 2 mm or more, microPET-CT with ^{18}F-FDG was performed to estimate metabolic volume. In case of radiopharmaceutical accumulation, we recognized mature tumor and followed-up evolution using ^{18}F-FDG and ^{18}F-FET alternately (one scanning per a day). MicroPET-CT with ^{18}F-FET was not performed in 2 animals from the 101.8 group due to technical reasons.

Two animals additionally underwent contrast-enhanced CT for comparison with MRI data and assessment of blood-brain barrier disruption. We performed ultra-high resolution CT with image reconstruction using voxel size 40×40×40 µm. Scanning area included only the head [10].

PET-SPECT-CT was performed using 3-modal preclinical device MiLabs VECTor6 (MiLabs, Netherlands) at the Blokhin National Cancer Research Center. The radiopharmaceutical was injected intravenously into the tail vein 5 min before scanning (137±26 MBq ^{18}F-FDG and 198±12 MBq ^{18}F-FET). Data collection period was 30 min. We used images averaged over the entire scan-

ning time. All quantitative measurements were performed in PMod 4.0 software (Switzerland).

Animals were withdrawn from the experiment after 18-day tumor growth. In histological examination, we analyzed mitotic figures, number of vessels and areas of necrosis under 200-fold magnification in at least 10 fields of view.

All procedures were conducted in accordance with the Helsinki Declaration (1964) and subsequent amendments thereto. In addition, the Bioethics Committee of the Research Institute for Experimental Diagnostics and Therapy of Tumors approved the study.

Results

Regardless of glioma model, radiopharmaceutical accumulation was either not observed (for small tumor sizes, **Fig. 1)** or was recorded when using both ^{18}F-FDG and ^{18}F-FET. This fact confirmed equivalence of any agent for working with glial models of brain tumors in rats. The ^{18}F-FET accumulation index was lower compared to ^{18}F-FDG only in one animal (rat #2, **Table 1)**. In all other cases, except for animals with 101.8 glioblastoma model #1 and #2, tyrosine accumulation index was equal or higher than ^{18}F-FDG accumulation index. At the same time, ^{18}F-FET standardized uptake value in intact brain was almost three times lower compared to similar value for ^{18}F-FDG (0.43±0.16 versus 1.26±0.20).

Comparison of glioma models regarding MRI and PET-CT parameters revealed differences in diagnostic characteristics of neoplasms **(Fig. 2)**.

Model 101.8 demonstrated large dimensions upon imaging (3—4 times larger than C6 tumor). This made it convenient to evaluate images and follow-up tumor evolution **(Table 1)**. All animals survived until the end of the experiment without any symptoms despite extensive central necrosis of tumor.

MRI visualized tumor as a compact node with heterogeneous structure, foci of small hemorrhages and cysts, as well as heterogeneous contrast enhancement. In all cases, PET-CT revealed central area with low rates of radiopharmaceutical accumulation that suggested central necrosis of tumor. Peripheral parts of tumor demonstrated active accumulation of radiopharmaceuticals.

There were no cases of spontaneous recovery or death of the animal before the end of the experiment in this model.

Model C6 turned out to be less stable in our experiment. In one animal (#1), the tumor ceased to be visualized by PET-CT over time despite baseline detectable metabolic activity. The 2nd animal with high metabolic activity of tumor (^{18}F-FET, T/N=3.3) was prematurely excluded from the experiment due to poor condition. Contrast-enhanced MRI demonstrated homogeneous tumors with multinodular growth in 2 cases. In all cases, PET-CT revealed compact distribution of radiopharmaceutical inside the tumor.

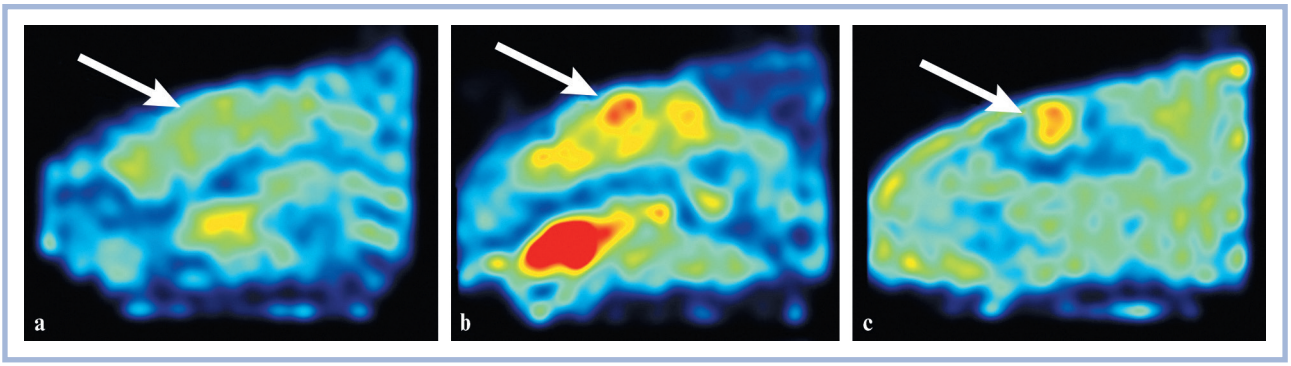


Fig. 1. **Experimental accumulation of various radiopharmaceuticals in the same animal (rat #4) with the 101.8 model. The arrow indicates the tumor.**
a — ^{18}F-FDG before appearance of metabolic activity in tumor; b — ^{18}F-FDG after active tumor growth; c — ^{18}F-FET accumulation the day after image "b" in the same animal; weak radiopharmaceutical accumulation in intact brain causes the pattern of reduced cerebral metabolism. Tumor is visible with greater contrast enhancement under low radiopharmaceutical accumulation in intact tissue. Images with ^{18}F-FDG (a, b) demonstrate radiopharmaceutical accumulation both in tumor (Fig. b) and brain tissue. Contrast enhancement of tumor is lower compared to other radiopharmaceutical. Additional accumulation of radiopharmaceutical in muscles of tongue allows it to be easily localized on PET/CT images.

Table 1. **Tumor parameters at the point of greatest growth as measured by ^{18}F-FDG microPET-CT (^{18}F-FET in brackets)**

Model C6	AI	Volume, mm^3	Model 101.8	AI	Volume, mm^3
#1	1.6 (1.6)	15	#1	1.4 (n/a)	99
#2	1.5 (3.3)	90	#2	1.3 (n/a)	104
#3	2.0 (1.6)	24	#3	1.6 (2.6)	240
#4	2.1 (2.1)	34	#4	1.4 (2.4)	142

Note. n/a — no data; AI — accumulation index.

Contrast-enhanced MRI demonstrated permeability of blood-brain barrier in tumor. In all cases, tumors intensively accumulated contrast agent that allowed clear detection in MR images and selection of animals for further PET-CT experiments. In 2 cases (model 101/8), we used microCT with X-ray contrast agent (Iopromide, 185 mg [I]/ml). Accumulation of this agent corresponded to MRI data and areas with high ^{18}F-FDG uptake **(Fig. 3)**. However, microCT was not widespread in our experiment due to long-term image acquisition with necessary continuous infusion of contrast agent and high fluid load. At the same time, this method may be used for experimental assessment of tumor topography in rats if specialized MRI is unavailable.

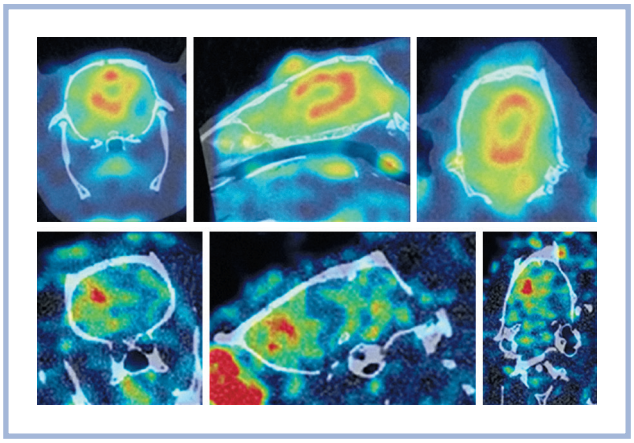


Fig. 2. **PET-CT in a rat with tissue model of glioblastoma 101.8 (upper row) and C6 (lower row).**
PET-CT demonstrates different patterns of ^{18}F-FDG accumulation in tumor tissue: peripheral type with central necrosis in 101.8 and compact type in C6 glioblastoma models (without central necrosis).

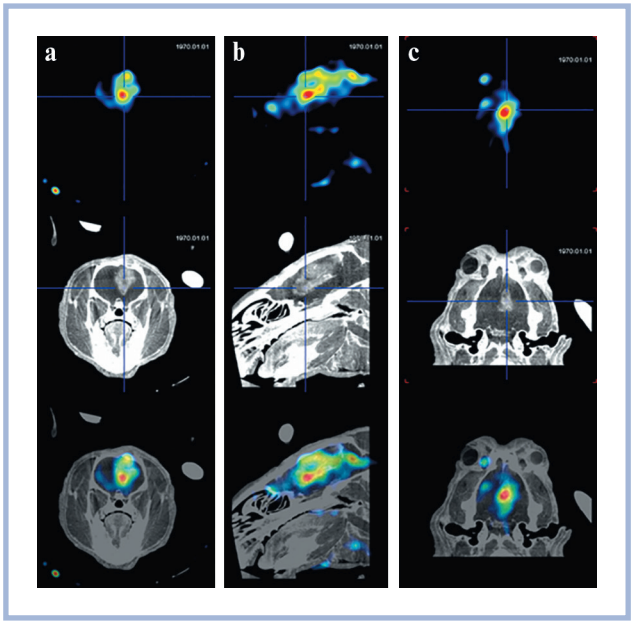


Fig. 3. **Animal #1. Tissue model of tumor 101.8.**
a — PET/CT with ^{18}F-FDG (upper row); b — frontal, sagittal and axial contrast-enhanced microCT scans; c — PET/CT. CT demonstrates a large tumor with heterogeneous contrast enhancement (center of line intersection); coincidence of metabolic activity in PET/CT and contrast-enhanced CT data on blood-brain barrier disruption. A bright focus in tumor (PET/CT scan) is an area of high cellularity, area of reduced density — necrosis.

In all cases, model 101.8 demonstrated high cellularity with polymorphic cells of various sizes, polymorphic nuclei and wide rim of cytoplasm **(Fig. 4b)**. Mitotic activity was high (5—6 mitoses per a field of view, ×200) **(Table 2)**. In addition, high vascularization was typical for this glioblastoma model. Vessels were characterized by disrupted architecture, thinned muscular wall and fenestrations. There were numerous pseudopalisade structures and necroses, and necrosis area was larger in central zone. Tumor border was relatively clear, but there were areas with diffuse tumor growth into surrounding intact tissues with cell growth along perineuronal and perivascular pathways. Astrocytic ridge along the tumor border was observed.

C6 glioma demonstrated high cellularity with fibrous component (cytoplasm-to-nucleus ratio 1:1) **(Fig. 4a)**. There were 3—4 mitotically dividing cells in a field of view (×200, **Table 2)**. Vascular component was represented by rare newly formed vessels of irregular shape. The number and area of necrosis differs significantly in central and peripheral parts of tumor. Only isolated small necroses were noted on tumor periphery in some cases. There was central necrosis in most cases. Moreover, necrosis area was significantly smaller compared to 101.8 model **(Table 2)**. There were no pseudopalisade structures. We observed clear tumor border with unclear astrocytic ridge, perineuronal and perivascular growth.

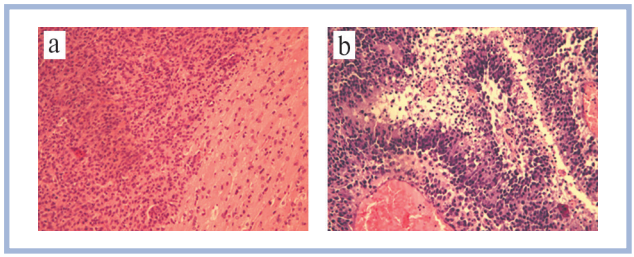


Fig. 4. **Histological analysis of tumor and contrast-enhanced MRI.**
a — C6 glioma; b — 101.8 glioma. Explanations in the text.

Table 2. **Morphometric indices of C6 and 101.8 gliomas after 18-day growth**

Model	Number of mitoses in a field of vision	Number of vessels in a field of vision (×200)	Necrosis area, % Me (25%; 75%)
C6	3—4	0—1	6.3 (3.2; 15.5)
101.8	5—6	8—12	32.6 (12.5; 55.8)

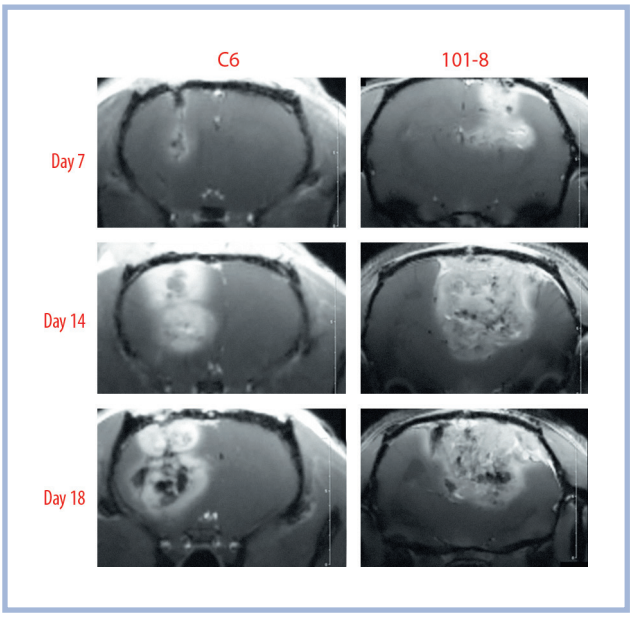


Fig. 5. **Contrast-enhanced T1WI of brains with gliomas 101.8 and C6 in 7, 14 and 18 days after tumor implantation.**
MRI demonstrates typical pattern of tumor growth (description in the text).

In 7 days after implantation, MRI visualized C6 glioma as a small tumor with weak contrast enhancement **(Fig. 5)**. After 14 days, we observed significant growth of tumor node. Moreover, 2 animals had 2 nodes with different contrast enhancement. After 18 days, significant growth of tumor occurred, and extensive central necrosis occurred in 1 case (#1). Other two cases demonstrated persistent compact contrast enhancement.

In 7 days after implantation of glioblastoma 101.8, we observed mature tumor nodes in all animals **(Fig. 5)**. Uneven accumulation of contrast agent indicated high tumor heterogeneity. There was significant tumor growth after 14 and 18 days without abruption of this process in any case. We observed heterogeneous tumor structure with multiple zones of small and medium-sized necroses.

Discussion

Currently, cell cultures of gliomas C6, F98, 9L and others for subcutaneous or intracranial experimental implantation are the most popular. These models are used in many fundamental studies, in particular, research of TSPO translation protein [11, 12], new radiopharmaceutical — [18F]VUIIS1018A, histone deacetylase enzymes (HDACs) [13], expression of σ2 receptors using a new radiopharmaceutical [18F]RM273 [14, 15], ALK2 receptor inhibitor for the treatment of diffusely growing pontine glioma [16]. All these researches are conducted on rats [17] and imply implantation of approximately 1 million cells into the animal's brain [18]. Modern radiopharmaceuticals demonstrate similar efficiency in visualization of experimental glioma [6, 19].

It is known that malignant tumor growth is directly related to its vascularization [20, 21]. Tumor vessels have abnormal morphology and architecture that ultimately leads to ischemia, hemorrhage, cell death and tumor necrosis [22—24]. Such processes are typical for malignant human gliomas and observed in glioblastoma 101.8.

The currently popular C6 glioma model did not demonstrate such tissue characteristics in our study. The tumor demonstrated no heterogeneity, extremely poor vascularization and low ability to form necrosis (with the exception of one case of extensive central necrosis after 18 days), as well as no pseudopalisade structures and tumor invasion typical for human glioblastoma.

On the other hand, tissue model 101.8 showed high heterogeneity of tumor structure, signs of neovascularization and invasion into surrounding tissues. In addition, neuroimaging and histological characteristics were similar to human glioblastoma.

Importantly, similar efficiency of PET-CT with ^{18}F-FDG and ^{18}F-FET in visualizing tissue models of glioma in rats justifies ^{18}F-FDG as more advisable and available agent in experimental researches.

Conclusion

Analysis of new tissue model 101.8 with PET/CT and MRI, as well as biopsy revealed its phenotypic and histological similarity with human glioblastoma. Features of tumor growth make it convenient for experimental studies using various neuroimaging methods. In our opinion, tissue model of glioblastoma 101.8 may be recommended to research groups testing new diagnostic and therapeutic drugs in experiments.

Funding
The study was supported by the Ministry of Science and Higher Education of the Russian Federation under agreement No. 075-15-2024-561.

Author contribution:
Concept and design of the study — Pronin I.N., Postnov A.A., Lipengolts A.A., Pavlova G.V., Grigorieva E.Yu., Alekseeva A.I.
Collection and analysis of data — Lipengolts A.A., Revishchin A.V., Skribitsky V.A., Finogenova Yu.A., Smirnova A.V., Shpakova K.E., Alekseeva A.I.
Statistical analysis — Postnov A.A.
Writing the text — Pronin I.N., Postnov A.A., Lipengolts A.A., Alekseeva A.I.
Editing — Pronin I.N., Postnov A.A., Finogenova Yu.A., Shpakova K.E., Alekseeva A.I.

The authors declare no conflicts of interest.

REFERENCES

1. Paolillo M, Comincini S, Schinelli S. In Vitro Glioblastoma Models: A Journey into the Third Dimension. *Cancers*. 2021;13(10):2449. https://doi.org/10.3390/cancers13102449
2. Sahu U, Barth RF, Otani Y, McCormack R, Kaur B. Rat and Mouse Brain Tumor Models for Experimental Neuro-Oncology Research. *Journal of Neuropathology and Experimental Neurology*. 2022;81(5):312-329. https://doi.org/10.1093/jnen/nlac021
3. Barth RF, Carpenter DE. Rodent Brain Tumor Models for Studies Focusing on Boron Neutron Capture Therapy. *Cancer Biotherapy and Radiopharmaceuticals*. 2023;38(3):148-151. https://doi.org/10.1089/cbr.2022.0041
4. Lenting K, Verhaak R, Ter Laan M, Wesseling P, Leenders W. Glioma: experimental models and reality. *Acta neuropathologica*. 2017;133(2):263-282. https://doi.org/10.1007/s00401-017-1671-4
5. Chu IR, Pan RL, Yang CS. Differentiation of Tumorigenic C6 Glioma Cells Induced by Enhanced IL-6 Signaling. *Medicina*. 2020;56(11):625. https://doi.org/10.3390/medicina56110625
6. Oliveira D, Stegmayr C, Heinzel A, Ermert J, Neumaier B, Shah NJ, Mottaghy FM, Langen KJ, Willuweit A. High uptake of 68Ga-PSMA and 18F-DCFPyL in the peritumoral area of rat gliomas due to activated astrocytes. *EJNMMI Research*. 2020;10(1):55. https://doi.org/10.1186/s13550-020-00642-0
7. Kolesnikova V, Revishchin A, Fab L, Alekseeva A, Ryabova A, Pronin I, Usachev DY, Kopylov A, Pavlova G. GQIcombi application to subdue glioma via differentiation therapy. *Frontiers in Oncology*. 2024;14:1322795. https://doi.org/10.3389/fonc.2024.1322795
8. Steiniger SC, Kreuter J, Khalansky AS, Skidan IN, Bobruskin AI, Smirnova ZS, Severin SE, Uhl R, Kock M, Geiger KD, Gelperina SE. Chemotherapy of glioblastoma in rats using doxorubicin-loaded nanoparticles. *International Journal of Cancer*. 2004;109(5):759-767. https://doi.org/10.1002/ijc.20048
9. Malinovskaya Y, Melnikov P, Baklaushev V, Gabashvili A, Osipova N, Mantrov S, Ermolenko Y, Maksimenko O, Gorshkova M, Balabanyan V, Kreuter J, Gelperina S. Delivery of doxorubicin-loaded PLGA nanoparticles into U87 human glioblastoma cells. *International Journal of Pharmaceutics*. 2017;524(1-2):77-90. https://doi.org/10.1016/j.ijpharm.2017.03.049
10. Patent RUS №2794034/11.04.2023. Byul. №11. Smirnova AV, Finogenova YuA, Varaksa PO, Lipengol'c AA, Skribickij VA, Lagodzinskaya YuS. *Method of introducing radiocontrast agents into the body of laboratory rodents for intravital radiation visualization of internal organs to assess the growth dynamics of malignant organotropic neoplasms in experimental oncology*. (In Russ.). https://www.fips.ru/iiss/document.xhtml?faces-redirect=true&id=496ec8163812b88614eb29e6e1372b26
11. Tang D, Li J, Nickels ML, Huang G, Cohen AS, Manning HC. Preclinical Evaluation of a Novel TSPO PET Ligand 2-(7-Butyl-2-(4-(2-[18F]Fluoroethoxy)phenyl)-5-Methylpyrazolo[1,5-a]Pyrimidin-3-yl)-N,N-Diethylacetamide (18F-VUIIS1018A) to Image Glioma. *Molecular Imaging and Biology*. 2019;21(1):113-121. https://doi.org/10.1007/s11307-018-1198-7
12. Tang D, Li J, Buck JR, Tantawy MN, Xia Y, Harp JM, Nickels ML, Meiler J, Manning HC. Evaluation of TSPO PET Ligands [18F]VUIIS1009A and [18F]VUIIS1009B: Tracers for Cancer Imaging. *Molecular Imaging and Biology*. 2017;19(4):578-588. https://doi.org/10.1007/s11307-016-1027-9
13. Laws MT, Bonomi RE, Kamal S, Gelovani DJ, Llaniguez J, Potukutchi S, Lu X, Mangner T, Gelovani JG. Molecular imaging HDACs class IIa expression-activity and pharmacologic inhibition in intracerebral glioma models in rats using PET/CT/(MRI) with [18F]TFAHA. *Scientific Reports*. 2019;9(1):3595. https://doi.org/10.1038/s41598-019-40054-2
14. Moldovan RP, Gündel D, Teodoro R, Ludwig FA, Fischer S, Toussaint M, Schepmann D, Wünsch B, Brust P, Deuther-Conrad W. Design, Radiosynthesis and Preliminary Biological Evaluation in Mice of a Brain-Penetrant 18F-Labelled σ2 Receptor Ligand. *International Journal of Molecular Sciences*. 2021;22(11):5447. https://doi.org/10.3390/ijms22115447
15. Wang T, Wang J, Chen L, Zhang X, Mou T, An X, Zhang J, Zhang X, Deuther-Conrad W, Huang Y, Jia H. Development of a Highly Specific 18F-Labeled Radioligand for Imaging of the Sigma-2 Receptor in Brain Tumors. *Journal of Medicinal Chemistry*. 2023;66(18):12840-12857. https://doi.org/10.1021/acs.jmedchem.3c00735
16. Murrell E, Tong J, Smil D, Kiyota T, Aman AM, Isaac MB, Watson IDG, Vasdev N. Leveraging Open Science Drug Development for PET: Preliminary Neuroimaging of 11C-Labeled ALK2 Inhibitors. *ACS Medicinal Chemistry Letters Journal*. 2021;12(5):846-850. https://doi.org/10.1021/acsmedchemlett.1c00127
17. Tang C, Nie D, Tang G, Gao S, Liu S, Wen F, Tang X. Radiosynthesis and biological evaluation of N-(2-[18F]fluoropropionyl)-3,4-dihydroxy-l-phenylalanine as a PET tracer for oncologic imaging. *Nuclear Medicine and Biology*. 2017;50:39-46. https://doi.org/10.1016/j.nucmedbio.2017.04.002
18. Alekseeva AI, Kudelkina VV, Kosyreva AM, Drozd SF, Gelperina SE, Pavlova GV, Khalansky AS. Nitric oxide donor nitrosorbide potentiates the antitumor effect of doxorubicin against experimental glioblastoma. *Burdenko's Journal of Neurosurgery*. 2022;86(1):66-73. (In Russ.). https://doi.org/10.17116/neiro20228601166
19. Stegmayr C, Bandelow U, Oliveira D, Lohmann P, Willuweit A, Filss C, Galldiks N, Lübke JH, Shah NJ, Ermert J, Langen KJ. Influence of blood-brain barrier permeability on O-(2-18F-fluoroethyl)-L-tyrosine uptake in rat gliomas. *European Journal of Nuclear Medicine and Molecular Imaging*. 2017;44(3):408-416. https://doi.org/10.1007/s00259-016-3508-0
20. Bergers G, Benjamin LE. Tumorigenesis and the angiogenic switch. *Nature reviews. Cancer*. 2003;3(6):401-410. https://doi.org/10.1038/nrc1093
21. Guelfi S, Hodivala-Dilke K, Bergers G. Targeting the tumour vasculature: from vessel destruction to promotion. *Nature reviews. Cancer*. 2024;24(10):655-675. https://doi.org/10.1038/s41568-024-00736-0
22. Kaur B, Khwaja FW, Severson EA, Matheny SL, Brat DJ, Van Meir EG. Hypoxia and the hypoxia-inducible-factor pathway in glioma growth and angiogenesis. *Neuro-oncology*. 2005;7(2):134-153. https://doi.org/10.1215/S1152851704001115
23. Domènech M, Hernández A, Plaja A, Martínez-Balibrea E, Balañà C. Hypoxia: The Cornerstone of Glioblastoma. *International journal of molecular sciences*. 2021;22(22):12608. https://doi.org/10.3390/ijms222212608
24. Steinbach JP, Wolburg H, Klumpp A, Probst H, Weller M. Hypoxia-induced cell death in human malignant glioma cells: energy deprivation promotes decoupling of mitochondrial cytochrome c release from caspase processing and necrotic cell death. *Cell death and differentiation*. 2003;10(7):823-832. https://doi.org/10.1038/sj.cdd.4401252

Received 15.09.2024
Accepted 20.09.2024

COMMENT

The authors compared morphophysiological and functional characteristics of two experimental models of glioma in rats.

The study is based on experiments on mature Wistar rats with intracranially implanted glioma samples. The authors analyzed tumor growth using MRI and PET/CT. Histological verification of tumors in animals was additionally carried out.

Both models demonstrated high similarity of metabolic activity compared to human glioblastoma. At the same time, MRI and histological examination revealed significant differences between the models. Model 101.8 had high similarity with spontaneous glioblastoma, while model C6 demonstrated significant disadvantages including low heterogeneity, accumulation and distribution of contrast agent different from spontaneous glioma, inadequate tissue necrosis in the follow-up period.

The authors' data allow us to agree with conclusions. However, the authors should take into account the following aspect. They present MR scans of different animals. Although this type of tumor is typical as mentioned, readers would be interested in observing the dynamics of tumor in a specific animal. Indeed, this would more specifically reflect appearance and development of necrotic zones.

This study has adequate experimental design. It is characterized by novelty, high potential for experimental neurooncology, as well as scientific and practical significance.

Galperina S.E. (Moscow)